Research Article

Nano Research
2023, 16(1): 1220–1227

ISSN 1998-0124 CN 11-5974/O4
https://doi.org/10.1007/s12274-022-4668-9

Robust n-type doping of WSe_2 enabled by controllable proton irradiation

Haidong Liang[1,3,§], Yue Zheng[2,3,§], Leyi Loh[4,§], Zehua Hu[6], Qijie Liang[7], Cheng Han[2], Michel Bosman[4] (✉), Wei Chen[3,5,8] (✉), and Andrew A. Bettiol[1,3] (✉)

[1] *Centre for Ion Beam Applications (CIBA), Department of Physics, National University of Singapore, Singapore 117542, Singapore*
[2] *International Collaborative Laboratory of 2D Materials for Optoelectronics Science and Technology of Ministry of Education, Institute of Microscale Optoelectronics, Shenzhen University, Shenzhen 518060, China*
[3] *Department of Physics, National University of Singapore, Singapore 117551, Singapore*
[4] *Department of Materials Science and Engineering, National University of Singapore, Singapore 117575, Singapore*
[5] *Department of Chemistry, National University of Singapore, Singapore 117543, Singapore*
[6] *Division of Physics and Applied Physics, School of Physical and Mathematical Science, Nanyang Technological University, Singapore 637371, Singapore*
[7] *Songshan Lake Materials Laboratory, Songshan Lake Mat Lab, Dongguan 523808, China*
[8] *National University of Singapore (Suzhou) Research Institute, 377 Lin Quan Street, Suzhou Industrial Park, Suzhou 215123, China*
[§] *Haidong Liang, Yue Zheng, and Leyi Loh contributed equally to this work.*

Received: 13 May 2022 / **Revised:** 9 June 2022 / **Accepted:** 15 June 2022

ABSTRACT

Two-dimensional (2D) transition metal dichalcogenides (TMDs) are considered to be promising building blocks for the next generation electronic and optoelectronic devices. Various doping schemes and work function engineering techniques have been explored to overcome the intrinsic performance limits of 2D TMDs. However, a reliable and long-time air stable doping scheme is still lacking in this field. In this work, we utilize keV ion beams of H_2^+ to irradiate layered WSe_2 crystals and obtain efficient n-type doping effect for all irradiated crystals within a fluence of 1×10^{14} protons·cm^{-2} (1e14). Moreover, the irradiated WSe_2 remains an n-type semiconductor even after it is exposed to ambient conditions for a year. Localized ion irradiation with a focused beam can directly pattern on the sample to make high performance homogenous p-n junction diodes. Raman and photoluminescence (PL) spectra demonstrate that the WSe_2 crystal lattice stays intact after irradiation within 1e14. We attribute the reliable electron-doping to the significant increase in Se vacancies after the proton irradiation, which is confirmed by our scanning transmission electron microscope (STEM) results. Our work demonstrates a reliable and long-term air stable n-type doping scheme to realize high-performance electronic TMD devices, which is also suitable for further integration with other 2D devices.

KEYWORDS

WSe_2, proton beam irradiation, n-type doping, long-time air stable, Se vacancies

1 Introduction

In recent years, two-dimensional (2D) transition-metal dichalcogenide (TMD) semiconductors have been considered ideal alternatives to Si for future-generation process nodes in semiconductor device fabrication due to their atomic-level thickness, good chemical stability and moderate bandgap [1–8]. Such unique properties make TMDs great platforms for electronics and optoelectronics, such as transistors, photodetectors, modulators and light-emitting diodes (LEDs) [9–12]. However, the unipolar transport property of most TMDs limits their applications, impeding their use in homogenous p-n junctions, diodes, and logic inverters. Therefore, various doping schemes and work function engineering techniques have been explored to modify the polarity of TMDs for functional devices [13–15].

One of the most commonly employed methods is interface engineering of TMDs with various organic/inorganic molecules or polymers to modulate their electrical and optoelectronic characteristics [16–32]. Various molecules or polymers can be selectively deposited into different interfaces (such as air/channel interface, metal/channel interface and dielectric/channel interface) to tune the interfacial properties of TMDs via a relatively facile process, realizing diverse functional devices in the homogenous flake. However, some of the deposited chemicals suffer from poor stability in air [20, 21, 26, 30], and hence can only be used in high vacuum conditions [21, 22], which greatly hinders their useful applications in microelectronic devices. In addition, a critical bottleneck of organic materials is their weak bonding and stability under high-temperature or chemical processing [16], which renders this doping route unsatisfactory for 2D semiconductors.

Physical modification methods, such as ion/electron beam irradiation, plasma etching, laser treatment and strain engineering [33–48], are also widely utilized to tailor the electrical and optical

Address correspondence to Michel Bosman, msemb@nus.edu.sg; Wei Chen, phycw@nus.edu.sg; Andrew A. Bettiol, a.bettiol@nus.edu.sg

properties of TMDs. However, most physical means are not only associated with poor controllability of defect types, but also cause potential lattice instability and even local destruction of the material. For example, ion irradiation and plasma etching usually produce a reduction in conductivity [49, 50], or even cause local deformation, irreversibly compromising the material property as a semiconductor [35–38, 40, 41, 47, 48]. Therefore, a robust doping technology with good controllability is highly sought after.

In this work, we demonstrate an efficient and reliable n-type doping scheme for naturally ambipolar WSe_2 by using 500 keV H_2^+ irradiation with an easily controlled fluence range (from 10^{13} (1e13) to 10^{14} protons·cm^{-2} (1e14)). This method is applicable to WSe_2 ranging from a thickness of a single to a few atomic layers, and the as-treated devices exhibit high stability even after one year of exposure to ambient conditions. We also show that further annealing after the proton irradiation can greatly increase the electron mobility from 3.4 to 30.9 cm^2·V^{-1}·s^{-1}, dramatically decreasing the Schottky barrier (SB) height. These properties of our doping method make it an ideal strategy for further realizing 2D TMD-based electronic and optoelectronic applications.

2 Experimental section

2.1 Device fabrication

Mono- and few-layer WSe_2 were firstly exfoliated onto a SiO_2/Si substrate via scotch tape. A layer of polymethylmethacrylate (PMMA) photoresist (A5 950 K) was subsequently spin-coated on the silicon substrate. A conventional e-beam lithography (EBL) process was employed for patterning of electrodes. Layers of 5 nm Pd and 60 nm Au were sequentially thermally deposited onto the sample, and then lifting off was performed after immersing in acetone for 1 h. An aluminium wire was then bonded between the patterned electrodes and the lead of the chip carrier, and the device was loaded into a high vacuum chamber for electrical measurements.

2.2 Raman and PL measurement

All Raman and PL measurements were performed in a commercial WITech system, where the incident laser wavelength was 532 nm and the power was fixed at 500 μW.

2.3 Ion irradiation

A SingletronTM accelerator was used to generate H_2^+ ion beams from a hydrogen source bottle at 500 kV terminal voltage. 500 keV H_2^+ was selected by controlling a 90-degree magnetic field.

Large area irradiation: The beam was roughly focused with a quadrupole lens set to a spot with a diameter of a few tens micrometers, and raster-scanned over an area of ~ 3 mm × 3 mm covering the whole WSe_2 flake. The irradiation fluence was controlled by the beam current and irradiation time. The beam current was tuned from less than 1 pA to several μA with a stability of ~ 3%. In this work, we used a beam current of around 1 nA for fluences 1e13–1e14 with irradiation time of several minutes.

Localized irradiation: The beam was focused to a spot with a diameter of ~ 100 nm, and controlled scanned over part of the WSe_2 sample.

2.4 Scanning transmission electron microscope (STEM) imaging and sample transfer

High-angle annular dark-field (HAADF)-STEM images were acquired with an aberration-corrected JEM-ARM200CF (JEOL) instrument equipped with a cold field emission gun and DCOR probe corrector, operated at 80 kV with a convergence angle of 31 mrad. Prior to imaging, ion-irradiated samples were picked up with polycarbonate (PC) on a polydimethylsiloxane (PDMS) stamp, positioned and subsequently adhered onto a holey silicon nitride TEM support membrane (Ted Pella, Inc.) with a PC film melted at 185 °C. The PC film was then removed in chloroform vapour at 120 °C, leaving the bare samples on the support membrane. The transferred samples were placed in vacuum overnight prior to imaging the next day to ensure that all the solvent was dried off.

3 Results and discussion

3.1 N-type doping of WSe_2 by proton irradiation

Monolayer and multilayer WSe_2 flakes were mechanically exfoliated on a heavily doped p-type silicon substrate with a 300 nm oxide top layer. The fabrication details of three-terminal WSe_2 field-effect transistor (FET) devices are discussed in the experimental section. In our experiments, all the electrical measurements were conducted under high vacuum conditions (~ 10^{-8} mbar). Figure 1(a) shows the optical microscope image (left) of the fabricated WSe_2 device. Two Pd/Au (5 nm/60 nm) electrodes were attached to the exfoliated WSe_2 flake as the source and drain, and 300 nm silicon dioxide served as the dielectric layer. The atomic force microscope (AFM) image (middle of Fig. 1(a)) shows a detailed morphology of the device, and the line profile (right of Fig. 1(a)) reveals that the thickness of the WSe_2 flake was about ~ 6 nm (~ 8 layers). Figure 1(b) exhibits the transfer transport characteristics (I_{sd}–V_g) of the WSe_2 FET before and after H_2^+ irradiation with different fluences at V_{sd} = 1 V in a logarithmic plot. For pristine devices, the source–drain current for the negative V_g sweeping side increased similarly to the positive side with the same magnitude, indicating bipolar transport of the FET. After H_2^+ irradiation with a fluence of 3 × 10^{13} protons·cm^{-2} (3e13, the fluence is calculated by proton numbers, 1 H_2^+ = 2 protons), the off state current moved to a lower gate voltage (about −35 V) with the current on/off ratio at the n-side increasing from ~ 10^5 to ~ 10^7. When the proton fluence was increased to 1e14, the gate voltage of the minimum current further negatively shifted to approximately −50 V; however the on/off ratio decreased to ~ 10^5. It is noteworthy that after the proton irradiation, the current for a positive V_g sweeping increased much faster than on the negative side and the threshold voltage (V_{th}) shifted negatively, which demonstrates clear n-type doping in the WSe_2. The field-effect mobility of WSe_2 can be evaluated with the equation below

$$\mu = \frac{L}{WC_iV_{sd}}\frac{dI_{sd}}{dV_g} \quad (1)$$

where dI_{sd}/dV_g represents the slope of the linear region in transfer plot; C_i represents the capacitance per unit area of the dielectric layer, while L and W are the length and width of the conduction channel, respectively. The carrier concentration can be estimated with the following equation

$$n = \frac{C_i(V_g - V_{th})}{e} \quad (2)$$

As shown in Fig. 1(c), the electron concentration n_e was continuously increased by ion irradiation from 0.75 × 10^{12} to 1.45 × 10^{12} cm^{-2} at V_g = 50 V due to the vacancies created by ion irradiation of the WSe_2, which will be discussed in detail later. Interestingly, the electron mobility μ_e increased from 0.5 to 1.8 cm^2·V^{-1}·s^{-1} with a proton fluence of 3e13, and then reduced to 1.3 cm^2·V^{-1}·s^{-1} with a fluence of 1e14. We propose that only few

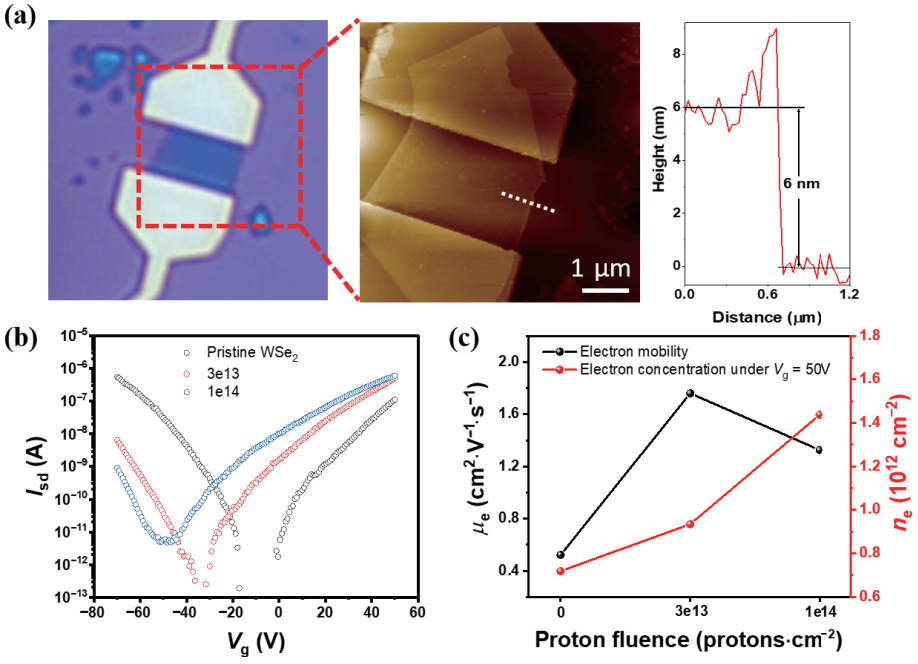

Figure 1 Electrical characterization of proton-modified WSe_2. (a) Optical image, AFM scan and corresponding thickness of few-layer WSe_2 FET. (b) Transfer characteristics under different proton fluences in a logarithmic plot. (c) The corresponding evolution of electron mobility and concentration.

atoms (W and Se) are knocked out and that the change to the overall crystal structure remains negligible when the proton fluence is low; therefore, the increase of the electron concentration lowers the SB at the contact region, raising the electrical potential at the channel region and resulting in the improvement of the calculated electron mobility. However, more vacancies are induced with a proton fluence of ~ 1e14 and the effect of lattice scattering outweighs the decrease of SB, leading to the observed reduction of the electron mobility.

3.2 Consistency and long-time air stability of the n-type doping effect

Despite the different thicknesses of the proton-irradiated WSe_2 flakes (1–10 layers) in our experiments, all of them were consistently n-type doped, as shown in Figs. S1(a)–S1(f) in the Electronic Supplementary Material (ESM). The threshold voltages were negatively shifted by more than 3 V, and the overall conductivity of WSe_2 under 50 V gate voltage was increased after ion irradiation in all cases (Fig. S1(f) in the ESM). In contrast to the previously-discussed chemical doping with molecules or polymers, our method shows superior stability in ambient conditions. Figure 2 displays the transfer characteristics of one bilayer sample before proton irradiation, after proton irradiation, and after one-year storage in a dry box. The off-state remained at the same V_g value after one year with an unchanged electrical conductivity at the electron side, indicating the stability of the n-type doping. However, at the hole regime, a significant increase of the conductivity was observed, which might originate from the absorption of water and oxygen during the air exposure [51]. Nevertheless, the irradiated WSe_2 can be transformed from a p-type to an n-type semiconductor with extremely high air stability as compared to previous works.

3.3 Optical characterizations

Raman spectroscopy was performed to study the crystal structure evolution before and after proton irradiation. As shown in Fig. 3(a), after proton irradiation with a fluence up to 1e14, the positions and the full widths at half-maximum (FWHM) of the characteristic Raman peaks of monolayer WSe_2 remained almost the same, indicating that the crystal lattice of the WSe_2 flake stayed intact after proton irradiation within the fluence of 1e14. Photoluminescence (PL) measurements of the monolayer WSe_2 before and after proton irradiation with different fluences were also carried out and shown in Fig. 3(b). The slight decrease in PL intensity for a proton fluence of 1e13 showed that a minor change of the crystal structure occurred for this fluence. When the proton fluence increased to 3e13, a reduction (~ 75%) of the PL intensity without any broadening of the PL peak can be observed. This

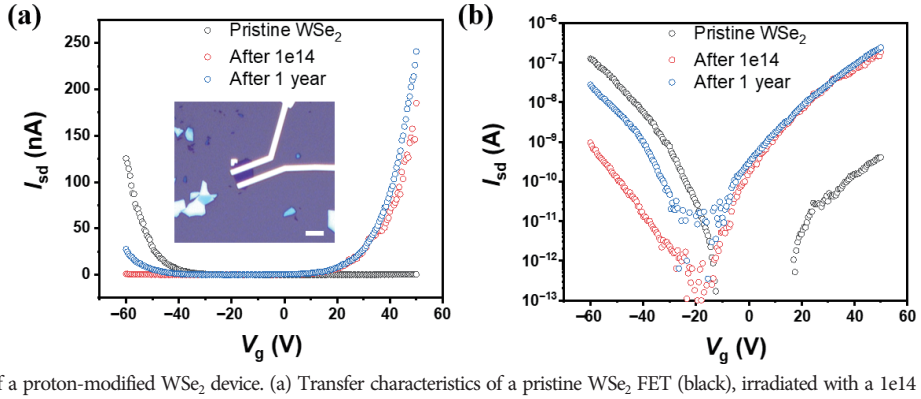

Figure 2 Air stability of a proton-modified WSe_2 device. (a) Transfer characteristics of a pristine WSe_2 FET (black), irradiated with a 1e14 proton fluence (red) and after 1-year air exposure (blue). Inset: optical image of the measured device, and scale bar: 5 μm. (b) The corresponding logarithmic *I*–*V* plot.

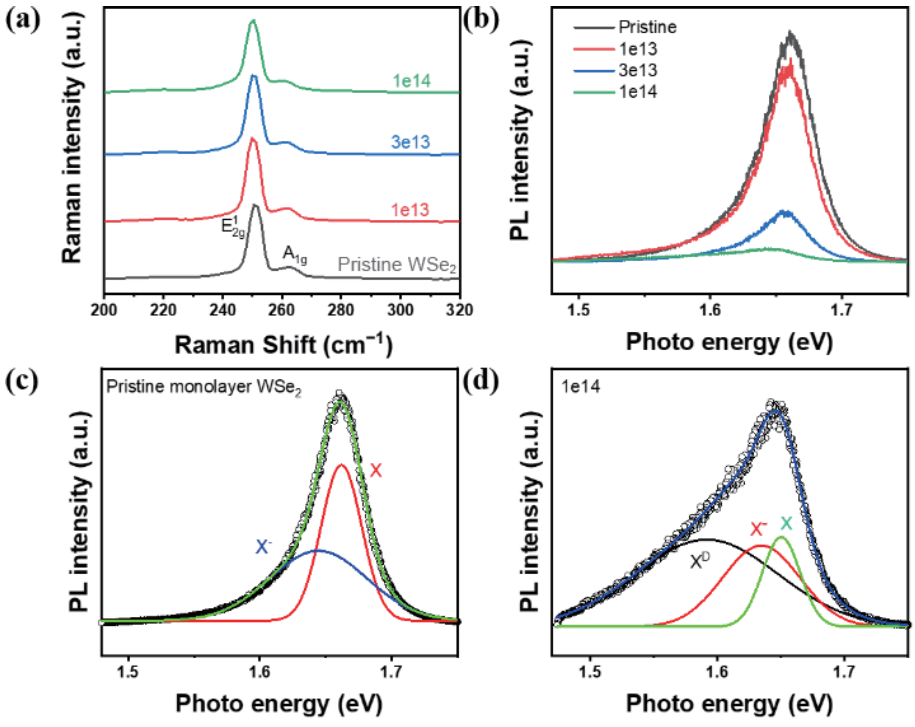

Figure 3 Optical characterization of monolayer WSe_2. (a) Raman spectra evolution with different proton fluences. (b) PL evolution with different proton fluences. Peak analysis of the PL spectra (c) for the pristine case and (d) for the 1e14 case.

could be a result of the creation of a large number of Se vacancies. As the proton fluence further increased to 1e14, the PL intensity continuously decreased down to less than 10% of the pristine PL intensity, with a significant FWHM broadening of the PL peak. Figure 3(c) shows the PL spectrum and a peak analysis of the pristine WSe_2, which is typical for an exfoliated monolayer WSe_2 as shown in previous reports [52–54]. The spectrum can be modelled by two Gaussian functions, corresponding to a neutral exciton X and a negatively-charged exciton X^- [55]. Figure 3(d) shows the PL spectrum and peak analysis of the same WSe_2 flake after proton irradiation with a fluence of 1e14. The spectrum can be modelled by three Gaussian functions. Besides the neutral and negatively charged exciton X and X^- as in the pristine case, another broad peak at lower energy emerges, which we attribute to the defects.

We also measured the optical spectra for higher fluences of 1e15 and 1e16. As shown in Fig. S2(a) in the ESM, the intensities of both E^1_{2g} and A_{1g} were reduced for a proton fluence of 1e15, and finally vanished at a fluence of 1e16, indicating that significant crystal lattice damage occurred. The PL spectra in Fig. S2(b) in the ESM reveal that after irradiation with a fluence of 1e15, most of the exciton emission was quenched by the proton irradiation, and only a very weak emission (~ 1% of the pristine PL) that corresponded to the defect peak (inset of Fig. S2(b) in the ESM) can be detected. Therefore, high fluence (over 1e15) proton irradiation induces severe damage to the crystal lattice. Alternatively, when the irradiation fluence stayed within 1e14, the overall crystal lattice remained intact and a well-controlled n-type doping can be consistently obtained for all the WSe_2 samples. Thus, controlling the irradiated fluence within a suitable range is crucial for obtaining stable n-doped WSe_2 flakes for functional devices.

3.4 Atomic structure characterizations with STEM

HAADF-STEM of a few-layer ion-irradiated WSe_2 sample reveals that the lattice still maintained a 2H configuration with no observable phase change (Figs. 4(a) and 4(b)). Due to the larger scattering cross section of W (atomic number 74) compared to a Se column (2 times atomic number 34 = 68), W atoms registered a marginally brighter signal with more electrons scattered to the HAADF detector (Fig. 4(b)). We identified two types of defects in our sample, namely the W vacancy (V_W) (Fig. 4(c)) and the Se vacancy (V_{Se}) (Fig. 4(d)). A strong signal drop in the presence of an atomic vacancy was more clearly visualized in the intensity plots in the bottom panels. From the large area HAADF-STEM image, we estimate V_{Se} to be higher than V_W and this is consistent across several other locations on the sample despite the significant densities of both defect types (Fig. S4 in the ESM). The V_W and V_{Se} densities in the irradiated WSe_2 are estimated to be 7.80×10^{12} and 1.72×10^{13} cm^{-2} respectively, significantly higher than those of the untreated WSe_2 which is estimated to have a V_W density of 1.28×10^{12} cm^{-2} and a V_{Se} density of 4.50×10^{12} cm^{-2} (Fig. S5 in the ESM). Although the increase in the density of V_{Se} is the highest (i.e., on the orders of ~ 10^{13} cm^{-2}) after beam treatment, it is also noteworthy that other minor point defects such as V_W, O substituents or even their defect complexes [56, 57] (i.e., present on the orders of ~ 10^{12} cm^{-2} or even less) can either compensate or have similar e-donating effect as V_{Se}, which will alter the effective e-donating ability by these V_{Se} defects. Nonetheless, we attribute V_{Se} to be the dominant defect type as a result of our ion-irradiation treatment. These V_{Se} defects act as electron donors for the initially ambipolar WSe_2, transforming it into an n-type semiconductor as illustrated in Fig. 1.

3.5 Annealing effect

As discussed previously, although proton irradiation can bring out non-volatile and long-term stable n-type doping for WSe_2, the creation of vacancies will increase the lattice scattering, which is detrimental to carrier transport in the channel. To ameliorate this, we subsequently annealed the device to reduce the lattice disorder due to proton irradiation. A WSe_2 multilayer (~ 10 layers) was first irradiated with protons with a fluence of 1e13, and subsequently annealed at 450 K under high vacuum (~ 10^{-7} mbar) for 5 h. Interestingly, the annealing process the n-type doping effect more pronounced (Fig. 5(a)) and the electron mobility enhancement increased from 2 times to 9 times (Fig. 5(b)). We

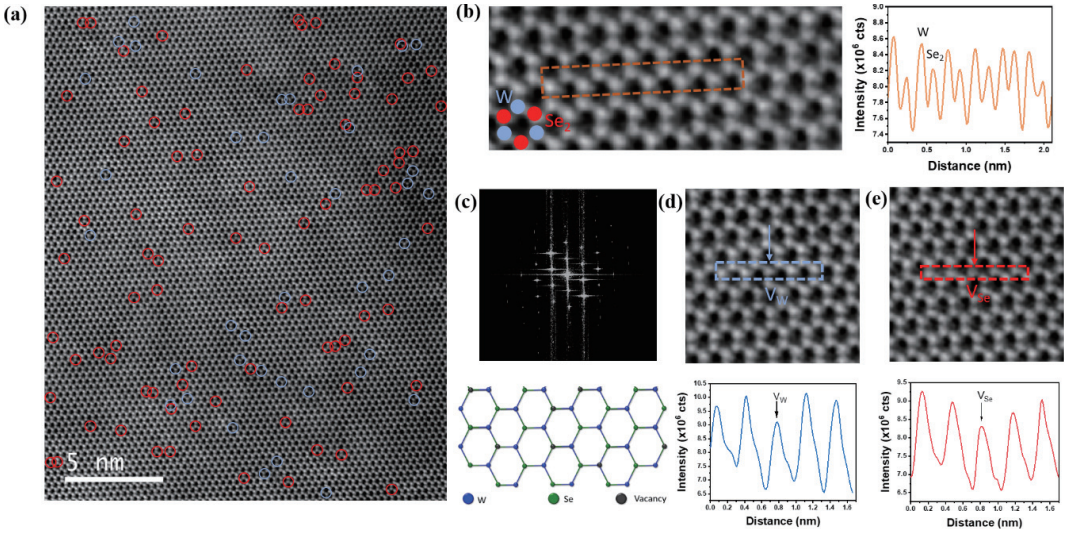

Figure 4 Atomic structure characterization of few-layer WSe_2 after 1e13 irradiation. (a) Large-area HAADF-STEM image of ion-irradiated few-layer WSe_2. The red and blue circles indicate the vacancies of Se and W, respectively. (b) Magnified HAADF-STEM image with the brown-striped area from which the integrated image intensity clearly shows that W columns are consistently brighter than Se_2 columns. (c) Fourier transform pattern based on the large area STEM image of irradiated WSe_2 with its corresponding atomic model. (d) W site vacancy and (e) Se vacancy as identified in the HAADF-STEM image and their respective intensity line scan.

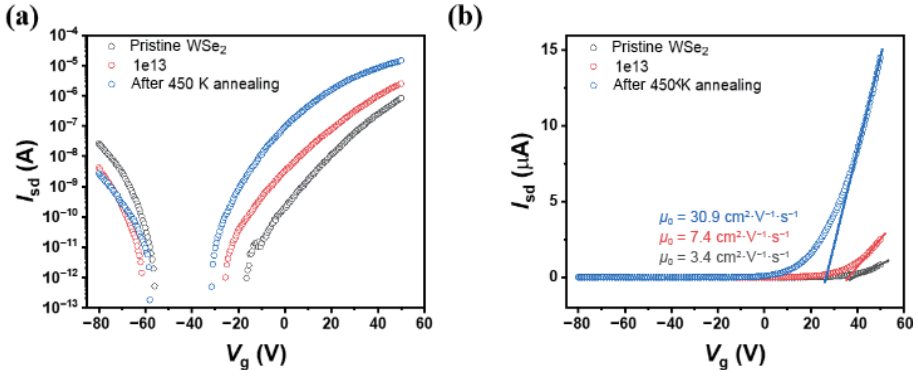

Figure 5 Comparison of a pristine WSe_2, WSe_2 after proton-modification, and WSe_2 after subsequent annealing. (a) Transfer characteristics of a pristine WSe_2 FET (black), the same WSe_2 after 1e13 proton fluence irradiation (red), and after subsequent annealing at 450 K (blue). (b) The corresponding linear plots with the measured electron mobilities indicated.

further conducted temperature-dependent experiments to explore the contact interfaces of the WSe_2 transistor under different conditions. Figures S6(a)–S6(c) in the ESM show the transfer characteristics of the transistor operated in vacuum at temperatures ranging from 77 to 300 K, respectively. According to the thermionic emission theory, the charge injection through the SB follows the equation below

$$I_{sd} = A^{*}_{2D} T^{\frac{3}{2}} \exp\left(-\frac{q\Phi_B}{k_B T}\right) \quad (3)$$

where A^{*}_{2D} and Φ_B represent the two-dimensional equivalent of the Richardson constant and the SB height, respectively. The SB height can be extracted from the Φ_B versus V_g plot when the flat band condition ($V_g = V_{FB}$) is satisfied, as shown in Figs. S6(g)–6(i) in the ESM. For a pristine sample, the SB height for electron injection is ~ 150 meV. The proton irradiation reduces the SB height to ~ 123 meV and further annealing decreases it to ~ 72 meV. Thus, proton irradiation can optimize the contact performance and further annealing can enhance this effect, which together provide a simple and effective method to obtain stable and high-performance n-type WSe_2.

3.6 Homogenous p-n junction diode formation by focused proton beam patterning

The electron doping effect by proton beams provides the possibility to form a homogenous WSe_2 lateral p-n junction diode. As shown in Fig. 6(a), a focused proton beam was precisely irradiated (with a fluence of 1e13) to a small region of a few-layer WSe_2 flake while the rest parts remained their pristine conduction properties. Three parallel electrodes were then deposited into the flake and marked as E1, E2 an E3. Figure 6(b) shows the *I*–*V* curves of these two lateral WSe_2 channels in linear scale and the optical image of the devices (inset). Interestingly, the untreated channel exhibited a near symmetry *I*–*V* character (Fig. 6(c)) while the partially irradiated channel demonstrated a rectifying behavior (Fig. 6(d)). The rectify ratio was over 10^4 and the ideality factor was about ~ 1.05, which is very close to the theoretical limitation ~ 1, revealing that our method can be used to effectively fabricate high-performance homogenous diodes.

4 Conclusion

In summary, we have demonstrated that high energy proton beam irradiation can consistently result in an n-type doping effect for monolayer and multilayer WSe_2 crystals with high stability in ambient conditions. PL and Raman spectroscopy showed that for proton irradiation fluence below 1e14, the crystal structure remained intact; however, higher fluences (> 1e15) resulted in severe damage to the lattice structure. STEM results confirmed that a large number of Se vacancies were created during proton irradiation that could serve as electron donors to increase the electron concentration in the material. Further thermal annealing

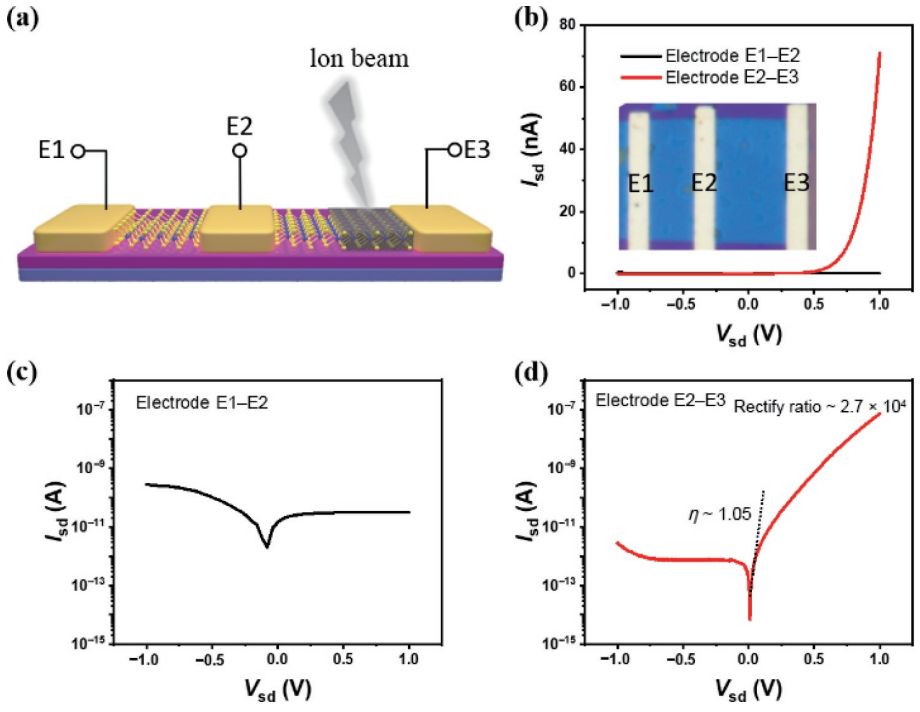

Figure 6 Localized proton modification for making homogenous diodes in WSe_2. (a) Schematic of the device and localized proton irradiation on the right side of the WSe_2 sample only covering the right electrode (E3) region. (b) *I*–*V* curves of the two WSe_2 channels in linear scale. The black line is measured between E1 and E2, and the red line between E2 and E3. (c) and (d) The corresponding logarithmic plots of the two different WSe_2 channels.

can make the n-type doping effect more pronounced and enhance the electron mobility with a reduction of the contact barrier. We can also use a focused proton beam for localized irradiation on part of WSe_2 to make homogenous diodes with high performance. Our results provide a non-volatile, long-term air stable and controllable strategy of n-type doping for WSe_2, which is also compatible with current complementary metal oxide semiconductor (CMOS) processes, and thus would be an ideal platform for future complementary high-performance electronics and optoelectronics applications. The presented method may be broadly applicable to other 2D TMDs as a simple, controllable method for generating n-type semiconductors.

Acknowledgements

The authors acknowledge financial support from NRF CRP on Oxide Electronics on Silicon Beyond Moore (NRF-CRP15-2015-01), the National Natural Science Foundation of China (Nos. U2032147, 21872100, and 62004128), Singapore MOE Grant T2EP50220-0001, MOE AcRF Tier 1 Startup grant R-284-000-179-133, the Science and Engineering Research Council of A*STAR (Agency for Science, Technology and Research) Singapore, under Grant No. A20G9b0135, and the Fundamental Research Foundation of Shenzhen (No. JCYJ20190808152607389).

Electronic Supplementary Material: Supplementary material (some more transfer characteristics, optical characterization and STEM results) is available in the online version of this article at https://doi.org/10.1007/s12274-022-4668-9.

References

[1] Wang, Q. H.; Kalantar-Zadeh, K.; Kis, A.; Coleman, J. N.; Strano, M. S. Electronics and optoelectronics of two-dimensional transition metal dichalcogenides. *Nat. Nanotechnol.* **2012**, *7*, 699–712.

[2] Wang, H.; Yu, L. L.; Lee, Y. H.; Shi, Y. M.; Hsu, A.; Chin, M. L.; Li, L. J.; Dubey, M.; Kong, J.; Palacios, T. Integrated circuits based on bilayer MoS_2 transistors. *Nano Lett.* **2012**, *12*, 4674–4680.

[3] Lee, Y. H.; Zhang, X. Q.; Zhang, W. J.; Chang, M. T.; Lin, C. T.; Chang, K. D.; Yu, Y. C.; Wang, J. T. W.; Chang, C. S.; Li, L. J. et al. Synthesis of large-area MoS_2 atomic layers with chemical vapor deposition. *Adv. Mater.* **2012**, *24*, 2320–2325.

[4] Lee, G. H.; Yu, Y. J.; Cui, X.; Petrone, N.; Lee, C. H.; Choi, M. S.; Lee, D. Y.; Lee, C.; Yoo, W. J.; Watanabe, K. et al. Flexible and transparent MoS_2 field-effect transistors on hexagonal boron nitride-graphene heterostructures. *ACS Nano* **2013**, *7*, 7931–7936.

[5] Akinwande, D.; Petrone, N.; Hone, J. Two-dimensional flexible nanoelectronics. *Nat. Commun.* **2014**, *5*, 5678.

[6] Liu, H.; Neal, A. T.; Ye, P. D. Channel length scaling of MoS_2 MOSFETs. *ACS Nano* **2012**, *6*, 8563–8569.

[7] Shi, Y. M.; Li, H. N.; Li, L. J. Recent advances in controlled synthesis of two-dimensional transition metal dichalcogenides via vapour deposition techniques. *Chem. Soc. Rev.* **2015**, *44*, 2744–2756.

[8] Chen, M. L.; Sun, X. D.; Liu, H.; Wang, H. W.; Zhu, Q. B.; Wang, S. S.; Du, H. F.; Dong, B. J.; Zhang, J.; Sun, Y. et al. A FinFET with one atomic layer channel. *Nat. Commun.* **2020**, *11*, 1205.

[9] Liu, Y.; Duan, X. D.; Huang, Y.; Duan, X. F. Two-dimensional transistors beyond graphene and TMDCs. *Chem. Soc. Rev.* **2018**, *47*, 6388–6409.

[10] Long, M. S.; Wang, P.; Fang, H. H.; Hu, W. D. Progress, challenges, and opportunities for 2D material based photodetectors. *Adv. Funct. Mater.* **2019**, *29*, 1803807.

[11] Sun, Z. P.; Martinez, A.; Wang, F. Optical modulators with 2D layered materials. *Nat. Photonics* **2016**, *10*, 227–238.

[12] Withers, F.; Del Pozo-Zamudio, O.; Mishchenko, A.; Rooney, A. P.; Gholinia, A.; Watanabe, K.; Taniguchi, T.; Haigh, S. J.; Geim, A. K.; Tartakovskii, A. I. et al. Light-emitting diodes by band-structure engineering in van der Waals heterostructures. *Nat. Mater.* **2015**, *14*, 301–306.

[13] Yoo, H.; Heo, K.; Ansari, H. R.; Cho, S. Recent advances in electrical doping of 2D semiconductor materials: Methods, analyses, and applications. *Nanomaterials* **2021**, *11*, 832.

[14] Luo, P.; Zhuge, F. W.; Zhang, Q. F.; Chen, Y. Q.; Lv, L.; Huang, Y.; Li, H. Q.; Zhai, T. Y. Doping engineering and functionalization of two-dimensional metal chalcogenides. *Nanoscale Horiz.* **2019**, *4*, 26–51.

[15] Loh, L.; Zhang, Z. P.; Bosman, M.; Eda, G. Substitutional doping in

2D transition metal dichalcogenides. *Nano Res.* **2021**, *14*, 1668–1681.
[16] Cho, K.; Pak, J.; Chung, S.; Lee, T. Recent advances in interface engineering of transition-metal dichalcogenides with organic molecules and polymers. *ACS Nano* **2019**, *13*, 9713–9734.
[17] Schmidt, H.; Giustiniano, F.; Eda, G. Electronic transport properties of transition metal dichalcogenide field-effect devices: Surface and interface effects. *Chem. Soc. Rev.* **2015**, *44*, 7715–7736.
[18] Kiriya, D.; Tosun, M.; Zhao, P. D.; Kang, J. S.; Javey, A. Air-stable surface charge transfer doping of MoS_2 by benzyl viologen. *J. Am. Chem. Soc.* **2014**, *136*, 7853–7856.
[19] Sim, D. M.; Kim, M.; Yim, S.; Choi, M. J.; Choi, J.; Yoo, S.; Jung, Y. S. Controlled doping of vacancy-containing few-layer MoS_2 via highly stable thiol-based molecular chemisorption. *ACS Nano* **2015**, *9*, 12115–12123.
[20] Kang, D. H.; Shim, J.; Jang, S. K.; Jeon, J.; Jeon, M. H.; Yeom, G. Y.; Jung, W. S.; Jang, Y. H.; Lee, S.; Park, J. H. Controllable nondegenerate p-type doping of tungsten diselenide by octadecyltrichlorosilane. *ACS Nano* **2015**, *9*, 1099–1107.
[21] Benjamin, C. J.; Zhang, S.; Chen, Z. H. Controlled doping of transition metal dichalcogenides by metal work function tuning in phthalocyanine compounds. *Nanoscale* **2018**, *10*, 5148–5153.
[22] Pak, J.; Jang, J.; Cho, K.; Kim, T. Y.; Kim, J. K.; Song, Y.; Hong, W. K.; Min, M.; Lee, H.; Lee, T. Enhancement of photodetection characteristics of MoS_2 field effect transistors using surface treatment with copper phthalocyanine. *Nanoscale* **2015**, *7*, 18780–18788.
[23] Mouri, S.; Miyauchi, Y.; Matsuda, K. Tunable photoluminescence of monolayer MoS_2 via chemical doping. *Nano Lett.* **2013**, *13*, 5944–5948.
[24] Li, Y.; Xu, C. Y.; Hu, P. A.; Zhen, L. Carrier control of MoS_2 nanoflakes by functional self-assembled monolayers. *ACS Nano* **2013**, *7*, 7795–7804.
[25] Dey, S.; Matte, H. S. S. R.; Shirodkar, S. N.; Waghmare, U. V.; Rao, C. N. R. Charge-transfer interaction between few-layer MoS_2 and tetrathiafulvalene. *Chem. -Asian J.* **2013**, *8*, 1780–1784.
[26] Kang, D. H.; Kim, M. S.; Shim, J.; Jeon, J.; Park, H. Y.; Jung, W. S.; Yu, H. Y.; Pang, C. H.; Lee, S.; Park, J. H. High-performance transition metal dichalcogenide photodetectors enhanced by self-assembled monolayer doping. *Adv. Funct. Mater.* **2015**, *25*, 4219–4227.
[27] Tarasov, A.; Zhang, S. Y.; Tsai, M. Y.; Campbell, P. M.; Graham, S.; Barlow, S.; Marder, S. R.; Vogel, E. M. Controlled doping of large-area trilayer MoS_2 with molecular reductants and oxidants. *Adv. Mater.* **2015**, *27*, 1175–1181.
[28] Andleeb, S.; Singh, A. K.; Eom, J. Chemical doping of MoS_2 multilayer by p-toluene sulfonic acid. *Sci. Technol. Adv. Mater.* **2015**, *16*, 035009.
[29] Ghimire, G.; Dhakal, K. P.; Neupane, G. P.; Jo, S. G.; Kim, H.; Seo, C.; Lee, Y. H.; Joo, J.; Kim, J. Optically active charge transfer in hybrids of Alq_3 nanoparticles and MoS_2 monolayer. *Nanotechnology* **2017**, *28*, 185702.
[30] Heo, K.; Jo, S. H.; Shim, J.; Kang, D. H.; Kim, J. H.; Park, J. H. Stable and reversible triphenylphosphine-based n-type doping technique for molybdenum disulfide (MoS_2). *ACS Appl. Mater. Interfaces* **2018**, *10*, 32765–32772.
[31] Peimyoo, N.; Yang, W. H.; Shang, J. Z.; Shen, X. N.; Wang, Y. L.; Yu, T. Chemically driven tunable light emission of charged and neutral excitons in monolayer WS_2. *ACS Nano* **2014**, *8*, 11320–11329.
[32] Yoo, H.; Hong, S.; Moon, H.; On, S.; Ahn, H.; Lee, H. K.; Kim, S.; Hong, Y. K.; Kim, J. J. Chemical doping effects on CVD-grown multilayer $MoSe_2$ transistor. *Adv. Electron. Mater.* **2018**, *4*, 1700639.
[33] Ghorbani-Asl, M.; Kretschmer, S.; Spearot, D. E.; Krasheninnikov, A. V. Two-dimensional MoS_2 under ion irradiation: From controlled defect production to electronic structure engineering. *2D Mater.* **2017**, *4*, 025078.
[34] Bertolazzi, S.; Bonacchi, S.; Nan, G. J.; Pershin, A.; Beljonne, D.; Samorì, P. Engineering chemically active defects in monolayer MoS_2 transistors via ion-beam irradiation and their healing via vapor deposition of alkanethiols. *Adv. Mater.* **2017**, *29*, 1606760.
[35] Mupparapu, R.; Steinert, M.; George, A.; Tang, Z.; Turchanin, A.; Pertsch, T.; Staude, I. Facile resist-free nanopatterning of monolayers of MoS_2 by focused ion-beam milling. *Adv. Mater. Interfaces* **2020**, *7*, 2000858.
[36] Madauß, L.; Ochedowski, O.; Lebius, H.; D'Etat, B. B.; Naylor, C. H.; Johnson, A. T. C.; Kotakoski, J.; Schleberger, M. Defect engineering of single- and few-layer MoS_2 by swift heavy ion irradiation. *2D Mater.* **2017**, *4*, 015034.
[37] Valerius, P.; Kretschmer, S.; Senkovskiy, B. V.; Wu, S. L.; Hall, J.; Herman, A.; Ehlen, N.; Ghorbani-Asl, M.; Grüneis, A.; Krasheninnikov, A. V. et al. Reversible crystalline-to-amorphous phase transformation in monolayer MoS_2 under grazing ion irradiation. *2D Mater.* **2020**, *7*, 025005.
[38] Choudhary, N.; Islam, M. R.; Kang, N.; Tetard, L.; Jung, Y.; Khondaker, S. I. Two-dimensional lateral heterojunction through bandgap engineering of MoS_2 via oxygen plasma. *J. Phys.: Condens. Matter* **2016**, *28*, 364002.
[39] Chen, Y.; Huang, S. X.; Ji, X.; Adepalli, K.; Yin, K. D.; Ling, X.; Wang, X. W.; Xue, J. M.; Dresselhaus, M.; Kong, J. et al. Tuning electronic structure of single layer MoS_2 through defect and interface engineering. *ACS Nano* **2018**, *12*, 2569–2579.
[40] Stanford, M. G.; Pudasaini, P. R.; Belianinov, A.; Cross, N.; Noh, J. H.; Koehler, M. R.; Mandrus, D. G.; Duscher, G.; Rondinone, A. J.; Ivanov, I. N. et al. Focused helium-ion beam irradiation effects on electrical transport properties of few-layer WSe_2: Enabling nanoscale direct write homo-junctions. *Sci. Rep.* **2016**, *6*, 27276.
[41] He, Z. Y.; Zhao, R.; Chen, X. F.; Chen, H. J.; Zhu, Y. M.; Su, H. M.; Huang, S. X.; Xue, J. M.; Dai, J. F.; Cheng, S. et al. Defect engineering in single-layer MoS_2 using heavy ion irradiation. *ACS Appl. Mater. Interfaces* **2018**, *10*, 42524–42533.
[42] Cheng, Z. H.; Abuzaid, H.; Yu, Y. F.; Zhang, F.; Li, Y. L.; Noyce, S. G.; Williams, N. X.; Lin, Y. C.; Doherty, J. L.; Tao, C. G. et al. Convergent ion beam alteration of 2D materials and metal-2D interfaces. *2D Mater.* **2019**, *6*, 034005.
[43] Jadwiszczak, J.; Keane, D.; Maguire, P.; Cullen, C. P.; Zhou, Y. B.; Song, H. D.; Downing, C.; Fox, D.; McEvoy, N.; Zhu, R. et al. MoS_2 memtransistors fabricated by localized helium ion beam irradiation. *ACS Nano* **2019**, *13*, 14262–14273.
[44] Komsa, H. P.; Kotakoski, J.; Kurasch, S.; Lehtinen, O.; Kaiser, U.; Krasheninnikov, A. V. Two-dimensional transition metal dichalcogenides under electron irradiation: Defect production and doping. *Phys. Rev. Lett.* **2012**, *109*, 035503.
[45] Gao, L.; Liao, Q. L.; Zhang, X. K.; Liu, X. Z.; Gu, L.; Liu, B. S.; Du, J. L.; Ou, Y.; Xiao, J. K.; Kang, Z. et al. Defect-engineered atomically thin MoS_2 homogeneous electronics for logic inverters. *Adv. Mater.* **2020**, *32*, 1906646.
[46] Stanford, M. G.; Pudasaini, P. R.; Gallmeier, E. T.; Cross, N.; Liang, L. B.; Oyedele, A.; Duscher, G.; Mahjouri-Samani, M.; Wang, K.; Xiao, K. et al. High conduction hopping behavior induced in transition metal dichalcogenides by percolating defect networks: Toward atomically thin circuits. *Adv. Funct. Mater.* **2017**, *27*, 1702829.
[47] Li, Z. Q.; Chen, F. Ion beam modification of two-dimensional materials: Characterization, properties, and applications. *Appl. Phys. Rev.* **2017**, *4*, 011103.
[48] Fox, D. S.; Zhou, Y. B.; Maguire, P.; O'Neill, A.; Ó'Coileaín, C.; Gatensby, R.; Glushenkov, A. M.; Tao, T.; Duesberg, G. S.; Shvets, I. V.; Abid, M. et al. Nanopatterning and electrical tuning of MoS_2 layers with a subnanometer helium ion beam. *Nano Lett.* **2015**, *15*, 5307–5313.
[49] Kim, T. Y.; Cho, K.; Park, W.; Park, J.; Song, Y.; Hong, S.; Hong, W. K.; Lee, T. Irradiation effects of high-energy proton beams on MoS_2 field effect transistors. *ACS Nano* **2014**, *8*, 2774–2781.
[50] Tosun, M.; Chan, L.; Amani, M.; Roy, T.; Ahn, G. H.; Taheri, P.; Carraro, C.; Ager, J. W.; Maboudian, R.; Javey, A. Air-stable n-doping of WSe_2 by anion vacancy formation with mild plasma treatment. *ACS Nano* **2016**, *10*, 6853–6860.
[51] Wang, S. F.; Zhao, W. J.; Giustiniano, F.; Eda, G. Effect of oxygen and ozone on p-type doping of ultra-thin WSe_2 and $MoSe_2$ field

effect transistors. *Phys. Chem. Chem. Phys.* **2016**, *18*, 4304–4309.
[52] Jones, A. M.; Yu, H. Y.; Ghimire, N. J.; Wu, S. F.; Aivazian, G.; Ross, J. S.; Zhao, B.; Yan, J. Q.; Mandrus, D. G.; Xiao, D. et al. Optical generation of excitonic valley coherence in monolayer WSe_2. *Nat. Nanotechnol.* **2013**, *8*, 634–638.
[53] Wang, Y. L.; Cong, C. X.; Yang, W. H.; Shang, J. Z.; Peimyoo, N.; Chen, Y.; Kang, J. Y.; Wang, J. P.; Huang, W.; Yu, T. Strain-induced direct-indirect bandgap transition and phonon modulation in monolayer WS_2. *Nano Res.* **2015**, *8*, 2562–2572.
[54] Zhu, C. R ; Zhang, K.; Glazov, M.; Urbaszek, B.; Amand, T.; Ji, Z. W.; Liu, B. L.; Marie, X. Exciton valley dynamics probed by Kerr rotation in WSe_2 monolayers. *Phys. Rev. B* **2014**, *90*, 161302(R).
[55] Ye, Y. X.; Dou, X. M.; Ding, K.; Jiang, D. S.; Yang, F. H.; Sun, B. Q. Pressure-induced *K–Λ* crossing in monolayer WSe_2. *Nanoscale* **2016**, *8*, 10843–10848.
[56] Zheng, Y. J.; Chen, Y. F.; Huang, Y. L.; Gogoi, P. K.; Li, M. Y.; Li, L. J.; Trevisanutto, P. E.; Wang, Q. X.; Pennycook, S. J.; Wee, A. T. S. et al. Point defects and localized excitons in 2D WSe_2. *ACS Nano* **2019**, *13*, 6050–6059.
[57] Zhang, S.; Wang, C. G.; Li, M. Y.; Huang, D.; Li, L. J.; Ji, W.; Wu, S. W. Defect structure of localized excitons in a WSe_2 monolayer. *Phys. Rev. Lett.* **2017**, *119*, 046101.